

Numerical study of electrical transport in co-percolative metal nanowire-graphene thin-films

Man Prakash Gupta, and Satish Kumar

Citation: *Journal of Applied Physics* **120**, 175106 (2016);

View online: <https://doi.org/10.1063/1.4965857>

View Table of Contents: <http://aip.scitation.org/toc/jap/120/17>

Published by the *American Institute of Physics*

Articles you may be interested in

[Evaluating conducting network based transparent electrodes from geometrical considerations](#)

Journal of Applied Physics **119**, 015102 (2016); 10.1063/1.4939280

[Predicting efficiency of solar cells based on transparent conducting electrodes](#)

Journal of Applied Physics **121**, 014502 (2017); 10.1063/1.4973117

[Investigation of phonon transport and thermal boundary conductance at the interface of functionalized SWCNT and poly \(ether-ketone\)](#)

Journal of Applied Physics **120**, 095102 (2016); 10.1063/1.4961604

[The effect of shallow vs. deep level doping on the performance of thermoelectric materials](#)

Applied Physics Letters **109**, 263902 (2016); 10.1063/1.4973292

[Electrical limit of silver nanowire electrodes: Direct measurement of the nanowire junction resistance](#)

Applied Physics Letters **108**, 163302 (2016); 10.1063/1.4947285

[Wettability transparency and the quasiuniversal relationship between hydrodynamic slip and contact angle](#)

Applied Physics Letters **108**, 074105 (2016); 10.1063/1.4942400



Scilight

Sharp, quick summaries **illuminating**
the latest physics research

Sign up for **FREE!**

AIP
Publishing

Numerical study of electrical transport in co-percolative metal nanowire-graphene thin-films

Man Prakash Gupta and Satish Kumar^{a)}

G. W. Woodruff School of Mechanical Engineering, Georgia Institute of Technology, Atlanta, Georgia 30332, USA

(Received 27 July 2016; accepted 7 October 2016; published online 4 November 2016)

Nanowires-dispersed polycrystalline graphene has been recently explored as a transparent conducting material for applications such as solar cells, displays, and touch-screens. Metal nanowires and polycrystalline graphene play synergetic roles during the charge transport in the material by compensating for each other's limitations. In the present work, we develop and employ an extensive computational framework to study the essential characteristics of the charge transport not only on an aggregate basis but also on individual constituents' levels in these types of composite thin-films. The method allows the detailed visualization of the percolative current pathways in the material and provides the direct evidence of current crowding in the 1-D nanowires and 2-D polygraphene sheet. The framework is used to study the effects of several important governing parameters such as length, density and orientation of the nanowires, grain density in polygraphene, grain boundary resistance, and the contact resistance between nanowires and graphene. We also present and validate an effective medium theory based generalized analytical model for the composite. The analytical model is in agreement with the simulations, and it successfully predicts the overall conductance as a function of several parameters including the nanowire network density and orientation and graphene grain boundaries. Our findings suggest that the longer nanowires (compared to grain size) with low angle orientation ($<40^\circ$) with respect to the main carrier transport direction provide significant advantages in enhancing the conductance of the polygraphene sheet. We also find that above a certain value of grain boundary resistance ($>60 \times$ intra-grain resistance), the overall conductance becomes nearly independent of grain boundary resistance due to nanowires. The developed model can be applied to study other emerging transparent conducting materials such as nanowires, nanotubes, polygraphene, graphene oxide, and their hybrid nanostructures. *Published by AIP Publishing.* [<http://dx.doi.org/10.1063/1.4965857>]

I. INTRODUCTION

Transparent conducting materials (TCMs) are used as electrodes in a wide range of applications such as solar cells, displays, photodetectors, touch-screens, and organic light-emitting diodes.^{1,2} Indium Tin Oxide (ITO) is currently the most commonly used TCM for these applications. However, due to increasingly high-cost and poor reliability over a period of time, there have been significant efforts towards finding alternative TCMs to replace ITO.^{2,3} Carbon nanotubes (CNTs), graphene, metal nanowires (NWs), and their hybrid nanostructures have been explored in this regard to achieve the desired combination of optimal material properties such as high optical transparency, high electrical conductivity, and greater mechanical flexibility.^{3–10}

Single-layer graphene is considered to have extremely high electrical conductivity (mobility $>200\,000\text{ cm}^2/\text{Vs}$) and very good optical transmittance (97.7% for visible light) while being a strong material in terms of mechanical flexibility.^{11,12} And therefore, ideally they would make an excellent candidate for replacement of ITO. However, the chemical

vapor deposition-grown large-scale graphene films are polycrystalline in nature with very high sheet resistance ($>1\text{ k}\Omega/\text{sq}$) due to several types of defects.^{13–17} In particular, the electrical transport between single-crystal domains (referred to as “grains”) in polygraphene is significantly influenced by scattering at the grain boundaries.^{18–20}

Recent theoretical and experimental studies have suggested that the transport properties of polygraphene can be significantly improved (sheet resistivity $<20\ \Omega/\text{sq}$; transparency $>90\%$ for visible light) by the addition of metallic NWs on polygraphene.^{21,22} The presence of NWs creates additional pathways over the grain boundaries which assist the charge carriers in overcoming the grain boundary resistance which increases the overall conductance.

While several useful electrical and optical measurements have been performed earlier to study these composites,^{22–25} there are various aspects of electrical transport in these materials, which require further detailed investigation such as: (1) how the NWs affect the local spatial variation of transport variables (e.g., current and potential) in polygraphene, (2) how the pathways for charge transport in polygraphene are altered by the NWs, (3) what is its dependence on the directional orientation of these NWs, and is there an optimal orientation to maximize macroscopic properties of these

^{a)}Author to whom correspondence should be addressed. Electronic mail: satish.kumar@me.gatech.edu

composites; and (4) how the local variation in the intrinsic and interfacial material properties affects the overall conductance. The numerical modeling approaches of these thin-film 1D/2D composites can be very helpful in answering these questions.

Some efforts have been made to model these composites but they are limited in terms of modeling the network of NWs and their interaction with graphene.^{21,26} There is a need to develop a physical model, which simultaneously describes the 1-D transport in NWs and 2-D transport in polygraphene. Such a model will provide greater details of the percolating nature of the charge transport in the NWs-polygraphene composites not only on an aggregate basis but also on individual constituents' levels. The model can also be used to extract material parameters (e.g., electrical conductivity of NWs, grain density in polygraphene, interfacial conductances, etc.) of these composites by comparing the simulation results with the experimental data. Furthermore, the model will serve as a precursor for the development of a self-consistent electro-thermal transport model for these composite thin-films, which can be used to study both electrical and thermal transport properties simultaneously. The computational framework developed here can be easily expanded to study the combination(s) of NWs, nanotubes, polygraphene and graphene oxide, all relevant as TCMs.²⁷

In the present work, we develop a comprehensive computational framework to simulate electrical transport in NW - polygraphene thin-film composites (Figure 1). The approach adopted here represents a better modeling technique for combined 1D-2D composites, compared to the ones presented in the previous studies^{21,26} as the governing equations are solved for both networks of 1-D NWs and 2-D polygraphene sheet. This approach allows the detailed visualization of the percolative current pathways in the material and provides the direct evidence of current crowding in the 1-D NWs and 2-D polygraphene sheet. This enables us to systematically study the effect of NW length, density, orientation, spatial distribution along with a host of other relevant material parameters such as grain boundary resistance, NW-graphene contact resistance, and grain size and density. Aside from the computational model and results, we also discuss an analytical model based on effective medium theories

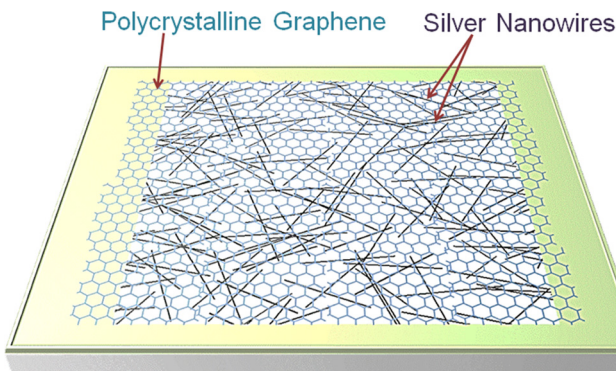


FIG. 1. Schematic representation of the 1D-2D composite of NWs-polygraphene thin-films.

for the combined nanowires-polygraphene composites. The analytical model can predict the overall conductance as a function of many parameters including the nanowire orientation and is in good agreement with the computational model.

II. METHODOLOGY

A. Computational framework

The shape of single crystal domains in polycrystalline graphene is typically non-uniform with stochastic variation.^{28,29} However, it has been reported that on average, sheet conductance of polygraphene is nearly independent of the grain-shape.²¹ Therefore, for simplicity, in this work we assume square grains. The grain size and NWs' length considered in the present study are sufficiently larger than the mean free path of charge carriers, and therefore charge transport can aptly be described by diffusive transport theory. This approximation has been validated and successfully applied in the case of carbon nanotube network based devices.³⁰⁻³² Governing equations are based on the charge conservation principle utilizing the diffusive transport theory. Equation (1) describes the charge transport in the ensemble of 1-D NWs, and it also includes the interaction among the NWs at the junctions and between NWs and polygraphene. Equation (2) describes the charge transport in the 2-D polygraphene sheet, and it also includes the interaction between the NW and the polygraphene

$$\frac{d^2\psi_i}{ds^2} + \tilde{G}_C(\psi_g - \psi_i) + \sum_{\substack{\text{intersecting} \\ \text{NWs } j}} \tilde{G}_{Jun}(\psi_j - \psi_i) = 0, \quad (1)$$

$$\nabla^2\psi_g + \sum_{i=1}^{N_{tubes}} \tilde{G}_C\beta_v(\psi_i - \psi_g) = 0, \quad (2)$$

where Ψ denotes the electric potential. All lengths are non-dimensionalized by the NW diameter (d). Ψ_i and Ψ_g denote the local potentials of the i th NW and polygraphene, respectively. The second and third terms in Equation (1) represent the charge transfer between NWs and polygraphene and at the NW junctions (if they intersect), respectively. \tilde{G}_C and \tilde{G}_{Jun} are non-dimensional contact conductance at NW-to-graphene and NW-to-NW contacts, respectively, defined as follows:^{33,34}

$$\tilde{G}_C = \frac{g_C P_C d^2}{\sigma_{NW} A}; \quad \tilde{G}_{Jun} = \frac{g_{Jun} P_{Jun} d^2}{\sigma_{NW} A};$$

$$\beta_v = \alpha_v \left(\frac{A}{P_S} \right) \frac{\sigma_{NW}}{\sigma_{Graphene}}.$$

Here, g_C and g_{Jun} are contact conductances per unit area at NW-to-graphene and NW-to-NW contacts, respectively; P_C and P_{Jun} are the corresponding contact perimeters. σ_{NW} and $\sigma_{Graphene}$ are the electrical conductivity of the NW and graphene, respectively. A is the cross-sectional area of the NW. The parameter β_v characterizes the contact geometry and α_v is the contact area per unit volume (area \times thickness) of the graphene cell. The polygraphene sample size ($L_x \times L_y$) is taken to be $52 \mu\text{m} \times 52 \mu\text{m}$ in the present study. The grain

size for most of the simulation results is considered to be $4\ \mu\text{m}$, consistent with the values reported in the literature.¹⁷ Each grain is further discretized into 10×10 cells. The boundaries at $x=0$ and $x=L_x$ are kept at 1 V and 0 V, respectively. Boundaries at $y=0$ and $y=L_y$ are considered to be periodic. It can be noted that the polygraphene sample size ($L_x \times L_y$) in the present simulations is more than ten times the grain size. This makes the simulation results expandable to much large sample sizes as well since the conductance is inversely proportional to the sample length (L_x) when $L_x > 10 L_{\text{grain}}$.²¹

Regarding the resistances of grain boundaries and within the grain, we adopt a similar approach as specified in Ref. 21. The intra-grain resistance of graphene is taken as $30\ \Omega/\text{sq}$ assuming only the acoustic deformation potential scattering.³⁵ The grain boundary resistance can vary in the polygraphene sheet, but for the present study we assume grain boundary resistance to be of binary nature, having either high or low resistance. Low resistance grain boundaries are considered to have the same resistance as the intra-grain resistance, while the high resistance grain boundaries are considered to have 60 times the resistance of intra-grain resistance. In the present study, we vary the percentage of high resistance grain boundaries as a parameter to study its effect on the transport properties of the Ag-NW/polygraphene thin-film. The location of the high resistance grain boundaries are randomly selected (Figure 2). The silver-NW length is considered to be $10\ \mu\text{m}$, diameter is $100\ \text{nm}$, nominal density is $6 \times 10^4/\text{mm}^2$, orientation distribution is random unless specified otherwise, and the electrical resistivity of the silver NW is taken as $2 \times 10^{-8}\ \Omega\ \text{m}$, consistent with the values reported in the literature.³⁶ The contact resistance (R_C) between the NW and graphene is considered to be $200\ \Omega\ \mu\text{m}$. The junction resistance between NWs is considered to be $10\ \Omega$.³⁶ Statistical averaging is performed over more than 100 ensembles of NW-polygraphene films for each data point to get rid the configuration bias

related to NW orientation and location of high and low resistance grain boundaries in polygraphene.

III. RESULTS AND DISCUSSION

A. Effect of NW density (D)

Figure 3 shows the contour plot results for electrostatic potential and current in the NWs and polygraphene sheet at two different values of NW density ($D = 1 \times 10^4/\text{mm}^2$ and $6 \times 10^4/\text{mm}^2$). The percentage of grain boundaries of high resistance is considered to be 60% for the two cases (Figures 3(a) and 3(e)). It can be noted that the potential map of the polygraphene sheet is dependent on the NW density such that the higher NW density helps reduce the spikes in the spatial gradient of potential caused by the high resistance grain boundaries (Figures 3(c) and 3(g)). Electric current variation and flow in the NWs and polygraphene for the two cases are shown in Figures 3(d) and 3(h)). These contour results provide the clear visualization of the percolation pathways and the resultant current crowding in both NWs and the polygraphene material caused by high resistance grain boundaries. We find that the location of high current regions in the polygraphene sheet is highly dependent on both the distribution of high resistance grain boundaries and NWs. Due to current crowding, high current is observed in parts of NWs located over the high resistance grain boundaries. Interestingly, not all NWs crossing over the high resistance grain boundaries possess high current segments. This is indicative of the fact that some NWs play more critical role than others, and a NW can have a variable effect on the overall conductance, depending on its environment. NWs that contribute to opening up the long-range percolating pathways for charge transport are more likely to play important role in enhancing the overall conductance. Higher density of NWs creates more low resistance percolating pathways in the polygraphene, which leads to higher current in the

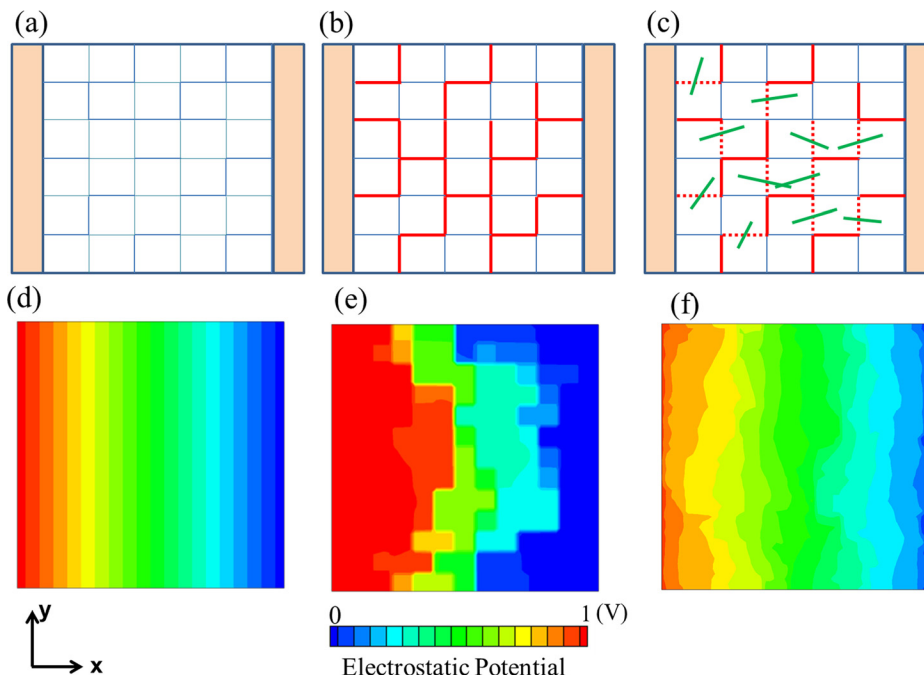


FIG. 2. Illustration of grain boundaries in (a) crystalline graphene, (b) polycrystalline graphene, and (c) NW-doped polycrystalline graphene, respectively. Charge transport gets impeded by high resistance grain boundaries (represented by red lines in (b)). NWs help increase the electrical conductance of polycrystalline graphene by providing the low resistance pathways over the grain boundaries. (d), (e), and (f) show the corresponding illustrative contour map of electrostatic potential for the above three cases, respectively. The NWs smoothen out the spikes in spatial gradient of potential caused by the grain boundaries.

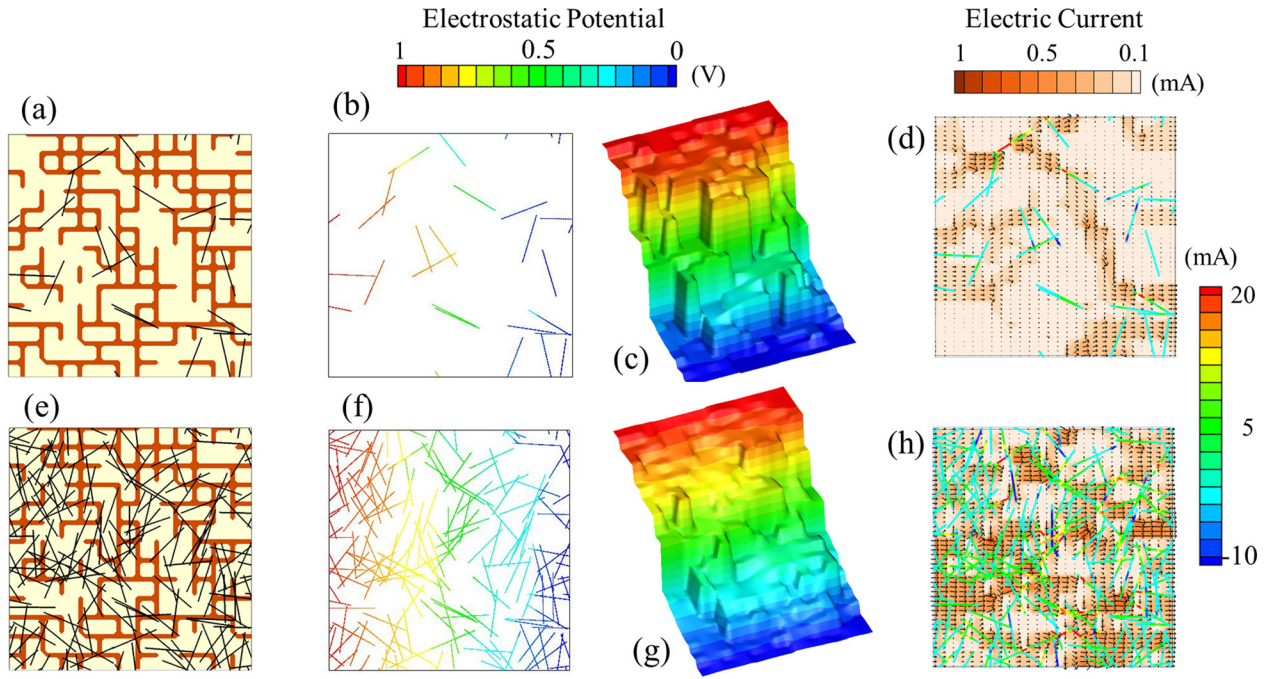


FIG. 3. Electrostatic potential and current distribution in NWs and polycrystalline graphene for two different NW density cases ($1 \times 10^4 / \text{mm}^2$ for the top row and $6 \times 10^4 / \text{mm}^2$ for the bottom row). (a) and (e) show the location of high resistance grain boundaries (60% of total) in polycrystalline graphene (red thick lines) and NWs (black thin lines). Higher density of NWs creates smoother potential profile and increases the current in the polygraphene sheet. Contour map of electrostatic potential of NWs (b) and (f) and polycrystalline graphene (c) and (g). Electric current in the NWs and polygraphene is shown together in (d) and (h) for two cases of NW density. High current in part of NWs (in red in d & h) clearly shows how they make bridge between clusters of graphene grains. Here, NWs are randomly oriented. Length of NW, $L_{\text{NW}} = 10 \mu\text{m}$ and grain size, $L_{\text{Grain}} = 4 \mu\text{m}$.

polygraphene sheet. Additional plots (Figures S2–S4) are included in the [supplementary material](#) for clarity in the current flow visualization corresponding to different cases of NW density and high resistance grain boundary percentages.

In order to explore the effect of NW density on overall conductance, we first discuss the nature of charge transport in the polygraphene material. We find that the electrical conductance of the poly-graphene sheet (without NWs) decreases by more than two orders of magnitude, changing it from a very good conductor to a poor conductor, when percentage of high resistance grain boundaries is increased from 0% to 100%. Particularly, a sharp drop is observed in the sheet conductance of polygraphene (for the zero NW density case in Figure 4) when the high resistance grain boundary percentage changes from 40% to 60%. This drop is a signature of percolation transport in the polygraphene. Above the percolation threshold of grain boundaries in polygraphene, the charges have to cross at least one high resistance grain boundary, and therefore the conductance decreases significantly. The addition of NWs alters the nature of charge percolation in polygraphene, as the NWs can effectively *short* the high resistance grain boundaries.

It is to be noted here that a separate percolation threshold exists for NW networks. The percolation threshold density for the NW network according to classical percolation theory for randomly oriented straight rods is given by $4.23^2 / \pi L_{\text{NW}}^2$, here L_{NW} is the NW length. For $L_{\text{NW}} = 10 \mu\text{m}$, the NW percolation threshold density is $5.7 \times 10^4 / \text{mm}^2$. We find that the NWs significantly benefit the polygraphene even when the NW density is below this network percolation threshold (Figure 4), since the charge transport through NW no longer requires their

interaction at the NW junctions. The increase in the conductance of polygraphene due to NWs is more pronounced when percentage of high resistance boundaries is higher, where even a small number of NWs can play significant role in enhancing the overall conductance. We find that higher density of NWs leads to greater overall conductance, albeit with diminishing returns. It can be seen here that it takes NW density of $9 \times 10^4 / \text{mm}^2$ to completely cancel the effect of 40% high resistance grain boundaries. More results regarding the statistical uncertainty due to ensemble averaging in the

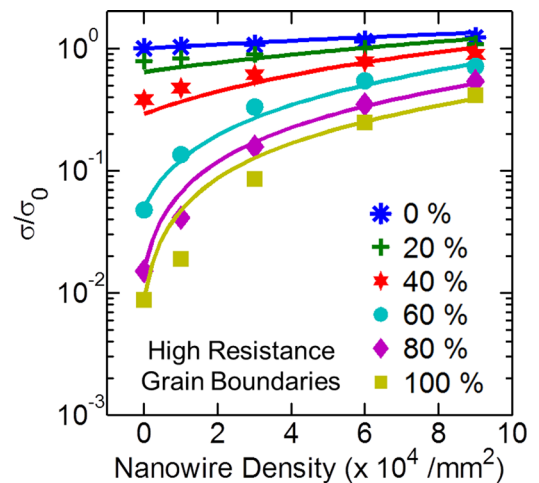


FIG. 4. Variation of normalized conductance of NW-assembled polygraphene with NW density (D) for different percentages of grain boundaries with high resistance. Here, $L_{\text{NW}} = 10 \mu\text{m}$, $L_{\text{Grain}} = 4 \mu\text{m}$. Symbols and solid lines correspond to computational and analytical results, respectively.

simulations are presented in the [supplementary material](#) (Figure S7).

It is worth pointing out here that high density can also adversely affect the optical transmittance of these materials, and therefore the NW density needs to be carefully selected.²²

The trend also matches well (see Figure 4) with the analytical results obtained from Maxwell-Garnett effective medium approximation (MG-EMA) theory, which is typically applied for finding the effective thermal conductance of fiber-reinforced matrix composites.^{37–39} Here, we are able to successfully apply MG-EMA theory (Equations (3)–(6)) to obtain effective electrical conductance of the NW-polygraphene thin-film owing to the similarity between the governing equations of diffusive thermal and electrical transport in such composites. In MG-EMA theory, the matrix phase of the composite is typically assumed to be homogeneous. Therefore, we first calculate the effective electrical conductivity of polygraphene (σ_{PG}) using general effective media (GEM) theory as a function of percentages of low and high resistance boundaries (Equation (5)) and subsequently utilize it in MG-EMA theory to obtain the effective electrical conductivity of the NWs-dispersed polygraphene composite

$$\sigma = \sigma_{PG} \left[\frac{1 + f[\beta_{11}(1 - L_{11})(1 - \langle \cos^2 \theta \rangle) + 2\beta_{33}L_{11}\langle \cos^2 \theta \rangle]}{1 - f[\beta_{11}L_{11}(1 - \langle \cos^2 \theta \rangle) + \beta_{33}L_{33}\langle \cos^2 \theta \rangle]} \right], \quad (3)$$

$$\langle \cos^2 \theta \rangle = \frac{\int \rho(\theta) \cos^2 \theta \sin \theta d\theta}{\int \rho(\theta) \sin \theta d\theta}. \quad (4)$$

Here, σ is the effective electrical conductivity of the NW-polygraphene thin-film composite. f is the area fraction of NWs, L_{ii} is the geometrical factor dependent on the NW aspect ratio, $\beta_{ii} = (\sigma_{ii} - \sigma_{PG})/[\sigma_{PG} + L_{ii}(\sigma_{ii} - \sigma_{PG})]$, $\sigma_{11} = \sigma_{22} = \sigma_{NW}/[1 + (2a_K \sigma_{NW}/\sigma_{PG} d)]$, and $\sigma_{33} = \sigma_{NW}/[1 + (2a_K \sigma_{NW}/\sigma_{PG} L_{NW})]$.^{37,39} Here, σ_{NW} is electrical conductivity of the NW, a_K is the Kapitza radius, which takes into account the contact resistance between NWs and graphene, axis 3 represents the longitudinal axis of the NWs, and axes 1 and 2 are the other two transverse axes of the NWs. The symbol θ denotes the orientation of a NW measured with respect to the x-direction and $\rho(\theta)$ is the normalized distribution function which describes the orientation of NWs. For the present study, the geometrical factors are $L_{11} = L_{22} = 0.5$, $L_{33} = 0$. The value of $a_K = 50$ nm, diameter of NW (d) = 100 nm, and length of the NW, $L_{NW} = 10 \mu\text{m}$.

In order to obtain the effective conductivity of polygraphene (σ_{PG}), we utilize general effective medium (GEM) theory.^{21,40}

$$f_{GB} \left[\frac{\sigma_{GB}^{1/t} - \sigma_{PG}^{1/t}}{\sigma_{GB}^{1/t} + \eta \sigma_{PG}^{1/t}} \right] + f_G \left[\frac{\sigma_G^{1/t} - \sigma_{PG}^{1/t}}{\sigma_G^{1/t} + \eta \sigma_{PG}^{1/t}} \right] = 0. \quad (5)$$

Here, f_{GB} and f_G are the fractions of area covered by grain boundaries and grains, respectively, such that $f_{GB} + f_G = 1$. σ_{GB} and σ_G are the conductivity of the grain boundary and graphene, respectively. The parameter t is a characteristic

exponent and η is dependent on the percolation threshold of the polygraphene sheet.⁴⁰ Here, t and η are taken as fitting parameters with the value of 1 and 1.2, respectively.

In the case of randomly oriented NWs, Equation (3) reduces to following form:

$$\sigma = \sigma_{PG} \left[\frac{2 + f[\beta_{11}(1 - L_{11}) + \beta_{33}(1 - L_{33})]}{2 - f[\beta_{11}L_{11} + \beta_{33}L_{33}]} \right]. \quad (6)$$

B. Effect of NW Alignment

Alignment of NWs on polygraphene determines the directional preference along which the grain boundaries are crossed over by the NWs. Given the stochastic spatial distribution of high resistance grain boundaries in polygraphene, it is important to understand how NW alignment affects the conductance of the composite. For this, we systematically change the orientation of NWs between 0° to 90° such that for a given orientation angle (θ), a NW's primary axis is allowed to make an angle of either θ or $-\theta$ with respect to the main direction of carrier transport. Figure 5 shows contour plots of electrostatic potential and electric current in NWs and polygraphene sheet for three different angle orientations ($\theta = 10^\circ, 60^\circ$, and 80°), for the case of 60% high resistance grain boundaries in polygraphene. Lower angle orientations of NWs lead to relatively smoother variation in the potential profile of polygraphene (Figures 5(c), 5(g), and 5(k)). It can be seen here that the orientation of NWs significantly influences which percolation pathways are reopened in the polygraphene sheet (Figures 5(d), 5(h), and 5(l)).

In the case of 10° alignment, we find that most of the NWs possess segments with high current as they crossover the high resistance grain resistance (Figure 5(d)). This indicates that most of the NWs are actively involved in suppressing the effect of high resistance grain boundaries and thereby increase the conductance. In the case of 80° orientation angle, NWs are oriented almost perpendicular to the direction of the applied electric field and do not contribute much to the opening up the percolating pathways in the relevant direction (Figure 5). Additional plots (Figures S5–S7) are included in the [supplementary material](#) for clarity in the current flow visualization corresponding to different cases of NW orientation and high resistance grain boundary percentages.

Next, we investigate the effect of NW alignment on the overall conductance at three different NW densities, $D = 1 \times 10^4, 3 \times 10^4$, and $6 \times 10^4 / \text{mm}^2$ (Figure 6). Figure 6(a) shows the alignment effect at different percentages of high resistance grain boundaries for density (D) = $1 \times 10^4 / \text{mm}^2$. At low percentages of high resistance grain boundaries (<40%), there are low resistance percolating pathways in polygraphene already available for charge transport. Therefore, the addition of NWs does not cause any appreciable change in the polygraphene sheet conductance and the orientation of these NWs also does not matter. However, for higher percentage (>40%) of high resistance grain boundaries, orientation of NWs starts affecting the sheet conductance significantly. Here, the maximum conductance is observed for low angle

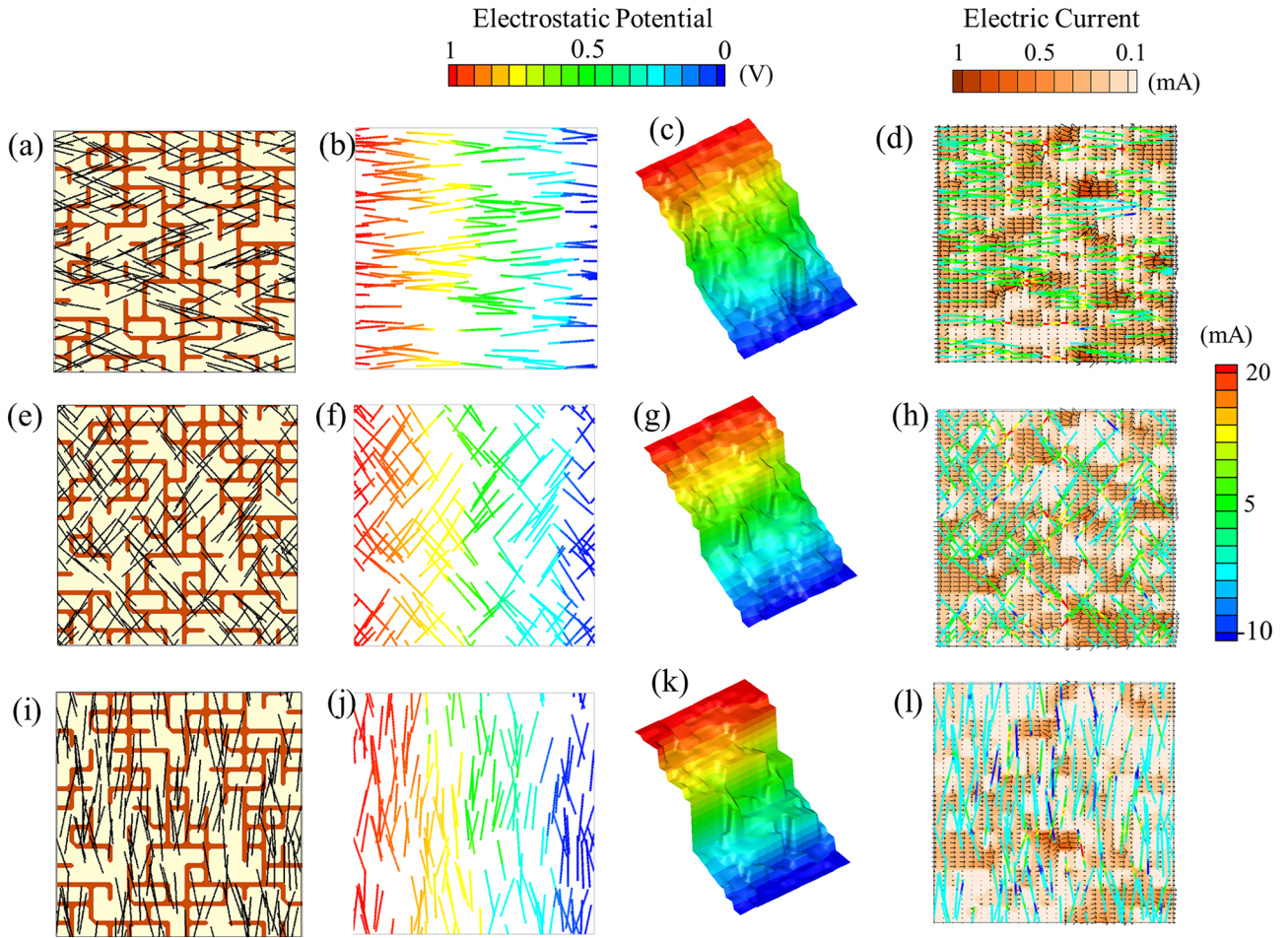


FIG. 5. Electrostatic potential and current distribution in NWs and polycrystalline graphene for three different NW alignment cases (10° for the top row, 60° for the middle row, and 80° for the bottom row). (a), (e), and (i) show the location of high resistance grain boundaries (60% of total) in polycrystalline graphene (red thick lines) and NWs (black thin lines). Contour map of electrostatic potential of NWs (b), (f), and (j) and polycrystalline graphene (c), (g), and (k). Electric current in the NWs and polygraphene is shown together in (d), (h), and (l) for the three alignment cases, respectively. Length of NW, $L_{NW} = 10 \mu\text{m}$ and grain size, $L_{\text{Grain}} = 4 \mu\text{m}$ and, NW density (D) = $6 \times 10^4 / \text{mm}^2$.

orientations ($\theta < 35^\circ$), and for high angle orientations conductance progressively decreases with the minimum observed at $\theta = 90^\circ$ when all the NWs are oriented perpendicular to the applied electric field (x-direction). It is worth repeating here that the length of NWs and grain size is $10 \mu\text{m}$ and $4 \mu\text{m}$, respectively. For low angle alignments, the one NW can only “short” a maximum of three grain boundaries. Under these conditions, it is less likely to have a complete low resistance percolating pathway for charge carriers at low NW density. Therefore, with $L_{NW} = 10 \mu\text{m}$ and $L_{\text{grain}} = 4 \mu\text{m}$, low NW density ($D = 1 \times 10^4 / \text{mm}^2$) does not significantly improve the conductance.

As the NW density is increased (Figures 6(b) and 6(c)), we find significant improvement in the sheet conductance at low alignment angles ($\theta < 40^\circ$) for high percentage (>60%) of high resistance grain boundaries. In the case of low angle ($\theta < 40^\circ$) orientations, NWs mainly cross the boundaries in the x-direction, and therefore, it creates greater chances of a complete low resistance pathway along the x-direction. Interestingly, a maximum is observed around $\theta = 20^\circ$ rather than at $\theta = 0^\circ$. Optimally angled NWs provide greater probability of crossing not only the high resistance boundaries in the

x-direction (vertical boundaries) but also in the y-direction (horizontal boundaries). This provides greater chances of a complete low resistance pathway across the sheet. We also find that the MG-EMA theory coupled with GEM theory for polygraphene is in good agreement with the computational results of the alignment effect of NWs (Figures 6(a)–6(c)). In the analytical model, the fitting parameter η assumes the values of 2, 3, and 4 (Equation (5)) corresponding to $D = 1 \times 10^4$, 3×10^4 , and $6 \times 10^4 / \text{mm}^2$, respectively. Increasing values of η is indicative of enhanced percolation threshold of the polygraphene caused by the addition of more NWs. More results regarding the statistical uncertainty due to ensemble averaging in the simulations are presented in the [supplementary material](#) (Figure S8).

The alignment effect is also dependent on the relative lengths of NWs and grains. In order to explore this dependence, we consider a case when the grain size is equal to the NW length ($L_{NW} = L_{\text{grain}} = 10 \mu\text{m}$) at $D = 6 \times 10^4 / \text{mm}^2$ (Figure 6(d)). In this case, efficacy of NWs in improving the conductance is reduced significantly despite high NW density as the NWs fail to “short” enough high resistance grain boundaries. Hence, the longer NWs ($> 2L_{\text{grain}}$) with low angle

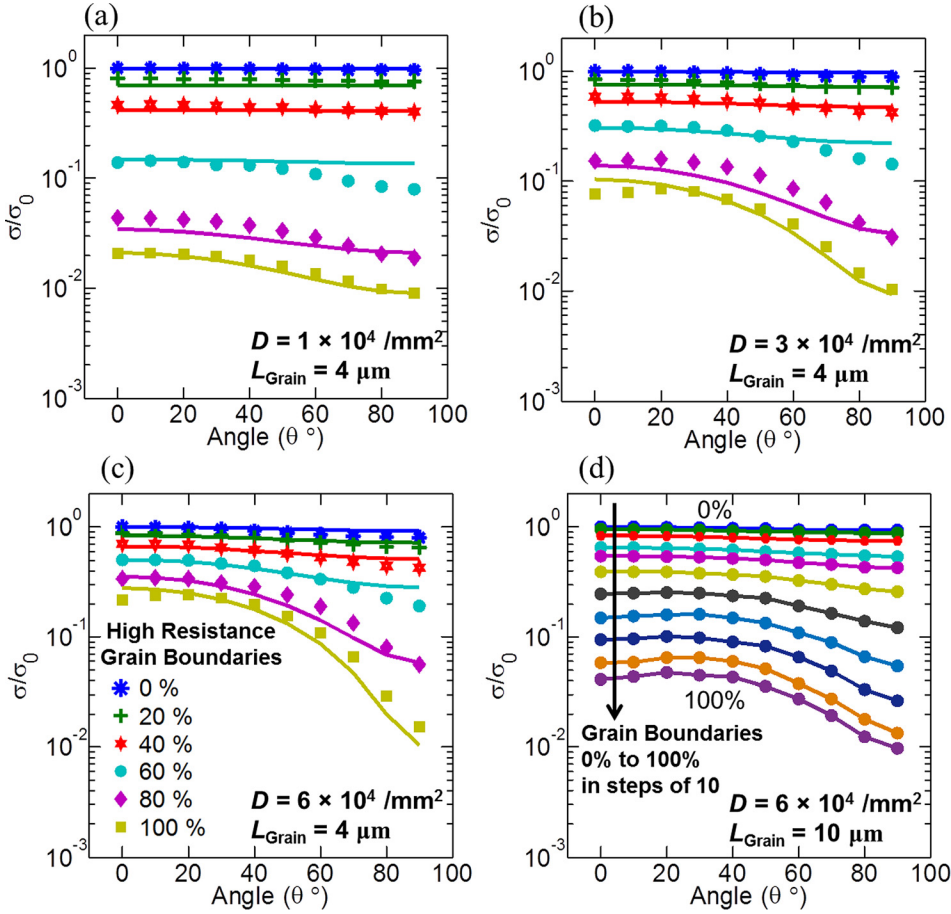


FIG. 6. Variation of normalized conductance of NW-doped polygraphene as a function of orientation of NWs for different values of the percentage grain boundaries. (a), (b), and (c) show the results from computational (symbols) and analytical (solid lines) models for NW density of 1×10^4 , 3×10^4 , and 6×10^4 /mm² where $L_{NW} = 10 \mu\text{m}$, $L_{\text{Grain}} = 4 \mu\text{m}$. (d) corresponds to the NW density of 6×10^4 /mm² and $L_{NW} = L_{\text{Grain}} = 10 \mu\text{m}$.

orientation ($<40^\circ$) with respect to the main carrier transport direction are favorable in enhancing the conductance of polygraphene sheet. We would like to add that the results, presented in this work, correspond to square grains and additional analysis can be performed for alternative grain shapes. We, however, speculate that the effect of grain shape distribution should not alter the nature of results discussed above as also found in Ref. 21.

The results discussed in the subsequent sections correspond to randomly oriented NWs.

C. Effect of graphene grain size (L_{Grain})

Figure 7 shows the effect of grain size on the conductance for a given NW length ($10 \mu\text{m}$). For comparison, three different grain sizes ($1 \mu\text{m}$, $2 \mu\text{m}$, and $4 \mu\text{m}$) are considered while keeping the NW length at $10 \mu\text{m}$. For smaller grain size, the number of grain boundaries increases, which leads to lower sheet conductance. The presence of NWs ($D = 6 \times 10^4$ /mm²) enhances the sheet conductance in all three cases but the overall conductance is different in all three cases, despite NW length and density being the same. This is due to the fact that a NW does not fully “short” the high resistance grain boundary. In order to understand it better, we further investigate the parameters which determine the interaction between NWs and graphene. This will help identify the fundamental limits to which NWs can improve the sheet conductance.

D. Effect of NW-graphene contact resistance (R_C)

The conductivity ratio of the NW and graphene ($\sigma_{NW}/\sigma_{\text{Graphene}}$) and the contact conductance (R_C) between the two determine the transport properties of the composite. We vary these two parameters to quantify their impact on the

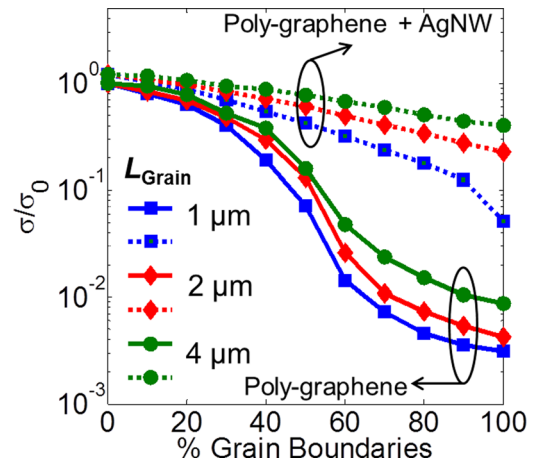


FIG. 7. Variation of normalized conductance of NW-doped polygraphene as a function of percentage high resistance grain boundaries for different size values of L_{NW}/L_{Grain} , here L_{NW} is the length of NW and L_{Grain} is the grain size. For the results shown here, L_{NW} is kept at $10 \mu\text{m}$ and L_{Grain} is varied between $1 \mu\text{m}$ and $4 \mu\text{m}$. Dotted and solid curves represent polygraphene conductance with and without NWs, respectively. The results shown are from simulations only.

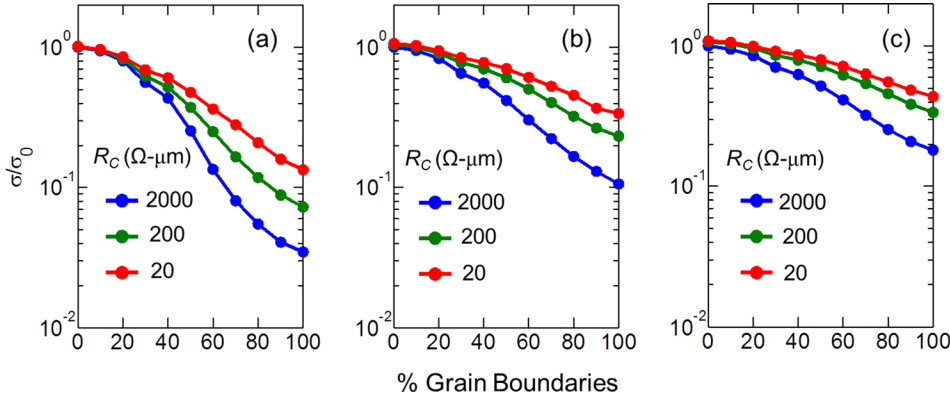


FIG. 8. Effect of NW-graphene contact resistance (R_C). Variation of normalized conductance of NW-doped polygraphene as a function of percentage grain boundaries for different values of R_C . (a), (b), and (c) correspond to $\sigma_{NW}/\sigma_{Graphene} = 0.45, 2.25,$ and 4.5 , respectively, where σ_{NW} and $\sigma_{Graphene}$ are electrical conductivity of the Ag NW and graphene, respectively. $L_{NW} = 10 \mu\text{m}$, $L_{grain} = 4 \mu\text{m}$. The results shown are from simulations only.

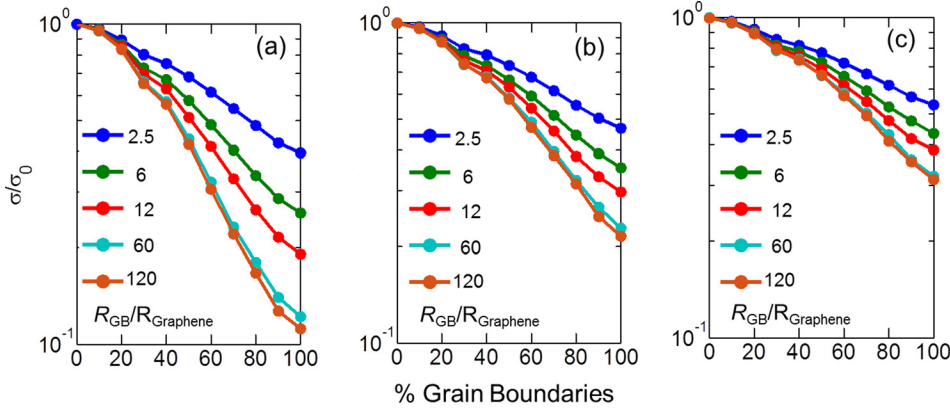


FIG. 9. Effect of grain boundary resistance ($R_{grain\ boundary}$). Variation of normalized conductance of NW-doped polygraphene as a function of percentage grain boundaries for different values of $R_{GB}/R_{Graphene}$. Here, $R_{Graphene}$ is the resistance of single grain of graphene with grain size of $4 \mu\text{m} \times 4 \mu\text{m}$. (a), (b), and (c) correspond to $R_C = 2000 \Omega\text{-}\mu\text{m}, 200 \Omega\text{-}\mu\text{m},$ and $20 \Omega\text{-}\mu\text{m}$, where R_C is NW-graphene contact resistance. NW density is $6 \times 10^4 / \text{mm}^2$. Here, $L_{NW} = 10 \mu\text{m}$, $L_{grain} = 4 \mu\text{m}$. The results shown are from simulations only.

conductance. Here, we consider three different values of $R_C = 20, 200,$ and $2000 \Omega\text{-}\mu\text{m}$. Three different values of $\sigma_{NW}/\sigma_{Graphene} = 0.45, 2.25,$ and 4.5 are considered (Figures 8(a)–8(c), respectively). Here, the intra-grain conductivity of the polygraphene sheet is calculated from intra-grain sheet resistance ($30 \Omega/\text{sq}$) taking the thickness to be 0.3 nm .

We find that the lower values of R_C lead to greater overall conductance for any given conductivity ratio $\sigma_{NW}/\sigma_{Graphene}$. However, in the case of $\sigma_{NW}/\sigma_{Graphene} = 0.45$, even a good electrical contact between the NW and polygraphene ($R_C = 20 \Omega\text{-}\mu\text{m}$) may become inadequate for the desired improvement in the sheet conductance.

It should be noted that the junction/interfacial resistances are treated as Ohmic (i.e., current across the interfaces is directly proportional to the potential difference). The results from Figure 8 can also be used to understand the possible non-linearity effects. If the interfacial resistance across the nanowire and graphene increases at higher bias due to the non-ohmic effects, the overall conductance will reduce. The degree to which it will affect the conductance will depend on the amount of increase in the interfacial resistance (R_C) and the conductance ratio of the nanowires and graphene ($\sigma_{NW}/\sigma_{Graphene}$) as indicated in Figure 8.

E. Effect of grain boundary resistance (R_{grain})

Another important parameter that affects the conductance of the polygraphene is the grain boundary resistance. In order to quantify its effect, we vary the grain boundary resistance for three different values of $R_C = 20, 200,$ and

$2000 \Omega\text{-}\mu\text{m}$ (Figure 9). For a given value of R_C , conductance of the composite decreases with increased grain boundary resistance. However, lower values of R_C diminish the adverse effects of grain boundary resistance; in other words, good quality of contacts between the NW and graphene ensures better charge transfer through the NW over the grain boundaries. In the case of very high grain boundary resistance, the current across the grain boundaries mainly flows through the NW pathways over the grain boundaries avoiding direct flow within the polygraphene across the grain boundaries. Therefore, we find that the increase in the grain boundary resistance beyond $R_{GB}/R_{Graphene} > 60$ does not lead to much further decrease in the sheet conductance of the composite. In such cases, the sheet conductance will be mainly be limited by the NW conductance.

Thus, the findings suggest that optimizing the values of different materials parameters including grain boundary resistance ($R_{GB}/R_{Graphene}$), the quality of the contact between the NW and graphene (R_C), and conductance of the NW (σ_{NW}) can significantly increase the conductance of NW-doped polygraphene thin-film composites which will improve their chances of potential usage in electronics and energy applications.

IV. CONCLUSION

In summary, we develop and employ a comprehensive computational model to study NW-doped polycrystalline graphene as the transparent conducting material for large-area applications. The sheet conductance of polycrystalline

graphene is greatly diminished due to the presence of grain boundaries. The presence of metal NWs on polygraphene creates pathways over the grain boundary to overcome the boundary resistance. We study the effect of various important parameters such as the NWs length, density and orientation, grain density in polygraphene, grain boundary resistance, and the contact resistance between the NW and graphene. The findings suggest that the longer NWs (compared to grain size) with low angle orientation ($<40^\circ$) with respect to the main carrier transport direction can be significantly advantageous in enhancing the conductance of the polygraphene sheet. We also find that above a certain value of grain boundary resistance ($>60 \times$ intra-grain resistance), the overall conductance becomes nearly independent of grain boundary resistance, as the NWs become the sole pathways for charge transport across the grain boundaries. Both the conductance of NWs and the contact quality between the NW and graphene are found to be one of the most important parameters that determine the efficacy of NWs in improving the sheet conductance. Insights gained from the present study will help in the design and fabrication steps to optimize the sheet conductance of polygraphene for large-area applications. The developed model can also be used to extract the material properties of such NW-polygraphene composites from the experimental data of sheet conductance. The analytical model based on effective medium theories is also presented considering the orientation of NWs, and the results obtained from analytical model agree well with the corresponding computational results. The computational framework developed here can be easily expanded to study the combination(s) of NWs, nanotubes, polygraphene and graphene oxide, all relevant as TCMS. Furthermore, the model will serve as a precursor for the future work on the development of a self-consistent electro-thermal transport model for these composite thin-films, which can be used to study both electrical and thermal transport properties simultaneously.

SUPPLEMENTARY MATERIAL

See [supplementary material](#) for detailed contour plots of electrical current flow corresponding to different cases of NW density and orientation at various percentages of high resistance grain boundaries, and figures of the statistical uncertainty in terms of normalized standard deviation of the conductance.

ACKNOWLEDGMENTS

Authors would like to thank Professor M. A. Alam at Purdue University for the useful discussions which led us to perform this study.

¹E. Fortunato, D. Ginley, H. Hosono, and D. C. Paine, *MRS Bull.* **32**(3), 242–247 (2007).

²K. Ellmer, *Nat. Photonics* **6**(12), 808–816 (2012).

³D. S. Hecht, L. B. Hu, and G. Irvin, *Adv. Mater.* **23**(13), 1482–1513 (2011).

⁴C. F. Guo, Q. H. Liu, G. H. Wang, Y. C. Wang, Z. Z. Shi, Z. G. Suo, C. W. Chu, and Z. F. Ren, *Proc. Natl. Acad. Sci. U. S. A.* **112**(40), 12332–12337 (2015).

⁵C. F. Guo, T. Y. Sun, Q. H. Liu, Z. G. Suo, and Z. F. Ren, *Nat. Commun.* **5**, 3121 (2014).

⁶J. J. Liang, L. Li, X. F. Niu, Z. B. Yu, and Q. B. Pei, *Nat. Photonics* **7**(10), 817–824 (2013).

⁷K. S. Kim, Y. Zhao, H. Jang, S. Y. Lee, J. M. Kim, K. S. Kim, J. H. Ahn, P. Kim, J. Y. Choi, and B. H. Hong, *Nature* **457**(7230), 706–710 (2009).

⁸L. Xiao, Z. Chen, C. Feng, L. Liu, Z. Q. Bai, Y. Wang, L. Qian, Y. Y. Zhang, Q. Q. Li, K. L. Jiang, and S. S. Fan, *Nano Lett.* **8**(12), 4539–4545 (2008).

⁹L. Cai, J. Z. Li, P. S. Luan, H. B. Dong, D. Zhao, Q. Zhang, X. Zhang, M. Tu, Q. S. Zeng, W. Y. Zhou, and S. S. Xie, *Adv. Funct. Mater.* **22**(24), 5238–5244 (2012).

¹⁰D. J. Lipomi, M. Vosgueritchian, B. C. K. Tee, S. L. Hellstrom, J. A. Lee, C. H. Fox, and Z. N. Bao, *Nat. Nanotechnol.* **6**(12), 788–792 (2011).

¹¹R. R. Nair, P. Blake, A. N. Grigorenko, K. S. Novoselov, T. J. Booth, T. Stauber, N. M. R. Peres, and A. K. Geim, *Science* **320**(5881), 1308–1308 (2008).

¹²S. V. Morozov, K. S. Novoselov, M. I. Katsnelson, F. Schedin, D. C. Elias, J. A. Jaszczak, and A. K. Geim, *Phys. Rev. Lett.* **100**(1), 016602 (2008).

¹³X. S. Li, Y. W. Zhu, W. W. Cai, M. Borysiak, B. Y. Han, D. Chen, R. D. Piner, L. Colombo, and R. S. Ruoff, *Nano Lett.* **9**(12), 4359–4363 (2009).

¹⁴X. Li, W. Cai, J. An, S. Kim, J. Nah, D. Yang, R. Piner, A. Velamakanni, I. Jung, E. Tutuc, S. K. Banerjee, L. Colombo, and R. S. Ruoff, *Science* **324**(5932), 1312–1314 (2009).

¹⁵K. Kim, S. Coh, C. Kisielowski, M. F. Crommie, S. G. Louie, M. L. Cohen, and A. Zettl, *Nat. Commun.* **4**, 2723 (2013).

¹⁶S. Bae, H. Kim, Y. Lee, X. Xu, J.-S. Park, Y. Zheng, J. Balakrishnan, T. Lei, H. Ri Kim, Y. I. Song, Y.-J. Kim, K. S. Kim, B. Ozyilmaz, J.-H. Ahn, B. H. Hong, and S. Iijima, *Nat. Nanotechnol.* **5**(8), 574–578 (2010).

¹⁷Q. Yu, L. A. Jauregui, W. Wu, R. Colby, J. Tian, Z. Su, H. Cao, Z. Liu, D. Pandey, D. Wei, T. F. Chung, P. Peng, N. P. Guisinger, E. A. Stach, J. Bao, S.-S. Pei, and Y. P. Chen, *Nat. Mater.* **10**(6), 443–449 (2011).

¹⁸O. V. Yazyev and S. G. Louie, *Nat. Mater.* **9**(10), 806–809 (2010).

¹⁹P. M. Ajayan and B. I. Yakobson, *Nat. Mater.* **10**(6), 415–417 (2011).

²⁰A. W. Tsen, L. Brown, M. P. Levendorf, F. Ghahari, P. Y. Huang, R. W. Havener, C. S. Ruiz-Vargas, D. A. Muller, P. Kim, and J. Park, *Science* **336**(6085), 1143–1146 (2012).

²¹C. W. Jeong, P. Nair, M. Khan, M. Lundstrom, and M. A. Alam, *Nano Lett.* **11**(11), 5020–5025 (2011).

²²B. Deng, P. C. Hsu, G. C. Chen, B. N. Chandrashekar, L. Liao, Z. Ayitimidu, J. X. Wu, Y. F. Guo, L. Lin, Y. Zhou, M. Aisijiang, Q. Xie, Y. Cui, Z. F. Liu, and H. L. Peng, *Nano Lett.* **15**(6), 4206–4213 (2015).

²³I. N. Kholmanov, C. W. Magnuson, A. E. Aliev, H. F. Li, B. Zhang, J. W. Suk, L. L. Zhang, E. Peng, S. H. Mousavi, A. B. Khanikaev, R. Piner, G. Shvets, and R. S. Ruoff, *Nano Lett.* **12**(11), 5679–5683 (2012).

²⁴H. O. Choi, D. W. Kim, S. J. Kim, S. B. Yang, and H. T. Jung, *Adv. Mater.* **26**(26), 4575 (2014).

²⁵T. L. Chen, D. S. Ghosh, V. Mkhitarian, and V. Pruneri, *ACS Appl. Mater. Inter.* **5**(22), 11756–11761 (2013).

²⁶R. Y. Chen, S. R. Das, C. Jeong, M. R. Khan, D. B. Janes, and M. A. Alam, *Adv. Funct. Mater.* **23**(41), 5150–5158 (2013).

²⁷S. Das, S. Sadeque, C. Jeong, R. Chen, M. Alam, and D. Janes, *Nanophotonics* **5**(1), 180–195 (2016).

²⁸P. Y. Huang, C. S. Ruiz-Vargas, A. M. van der Zande, W. S. Whitney, M. P. Levendorf, J. W. Kevek, S. Garg, J. S. Alden, C. J. Hustedt, Y. Zhu, J. Park, P. L. McEuen, and D. A. Muller, *Nature* **469**(7330), 389 (2011).

²⁹P. Nemes-Incze, K. J. Yoo, L. Tapasztó, G. Dobrik, J. Labar, Z. E. Horvath, C. Hwang, and L. P. Biro, *Appl. Phys. Lett.* **99**(2), 023104 (2011).

³⁰S. Kumar, N. Pimparkar, J. Y. Murthy, and M. A. Alam, *Appl. Phys. Lett.* **88**(12), 123505 (2006).

³¹S. Kumar, N. Pimparkar, J. Y. Murthy, and M. A. Alam, *J. Appl. Phys.* **109**(1), 014315 (2011).

³²M. P. Gupta, L. Chen, D. Estrada, A. Behnam, E. Pop, and S. Kumar, *J. Appl. Phys.* **112**(12), 124506 (2012).

³³S. Kumar, N. Pimparkar, J. Y. Murthy, and M. A. Alam, *J. Appl. Phys.* **109**(1), 014315 (2011).

³⁴S. Kumar, M. A. Alam, and J. Y. Murthy, *Appl. Phys. Lett.* **90**(10), 104105 (2007).

³⁵J. H. Chen, C. Jang, S. D. Xiao, M. Ishigami, and M. S. Fuhrer, *Nat. Nanotechnol.* **3**(4), 206–209 (2008).

³⁶A. T. Bellew, H. G. Manning, C. G. da Rocha, M. S. Ferreira, and J. J. Boland, *ACS Nano* **9**(11), 11422–11429 (2015).

³⁷C. W. Nan, R. Birringer, D. R. Clarke, and H. Gleiter, *J. Appl. Phys.* **81**(10), 6692–6699 (1997).

³⁸S. Kumar, M. A. Alam, and J. Y. Murthy, *Appl. Phys. Lett.* **90**(10), 104105 (2007).

³⁹C. W. Nan, G. Liu, Y. H. Lin, and M. Li, *Appl. Phys. Lett.* **85**(16), 3549–3551 (2004).

⁴⁰D. S. McLachlan, M. Blaszkiewicz, and R. E. Newnham, *J. Am. Ceram. Soc.* **73**(8), 2187–2203 (1990).